Lab on a Chip

PAPER

View Article Online
View Journal

Cite this: DOI: 10.1039/d5lc00234f

Modular bioreactor for multi-well electrical stimulation of *in vitro* cardiac tissue engineering constructs

Suh Hee Cook, †[a] Jack Twiddy, †[b] Yuan Li,[c] Kiran M. Ali,[a] Daxian Zha,[a] Kaleah Gaddy,[a] Lauren Mabe,[b] Ke Huang,[d] Ke Cheng,[e] Michael A. Daniele[bf] and Jessica M. Gluck *[ab]

Systems for providing electrical stimulation to *in vitro* cell cultures are valuable in many tissue engineering applications. We designed and fabricated a novel modular bioreactor consisting of a printed circuit board assembly and carbon paper electrodes which is compatible with commercially available 12-well plates. Our system is the first low-cost, accessible bioreactor of its kind and capable of simultaneously supplying four different amplitudes of stimulus waveform to different wells of the bioreactor. SPICE and FEA were used to model and validate the delivery of these stimuli to cells in culture. We then used our bioreactor to apply 0 V, 0.1 V, 1 V, and 10 V of electrical stimulation to neonatal rat cardiomyocytes (NRCMs), with and without neonatal rat ventricular fibroblast co-culture, for 10 minutes daily on 7 consecutive days. Electrically stimulated NRCMs maintained viability except in response to 10 V stimulation in the absence of fibroblast co-culture. Furthermore, NRCMs exposed to 0.1 V stimulation exhibited enhanced markers (sarcomeric α-actinin and connexin 43) and upregulated genes (*βMYC*, *cTnI*, *Cav1*, and *Cx43*) related to cardiac electrophysiology compared to non-stimulated controls. This suggests 0.1 V stimulation with our bioreactor is advantageous for the electrophysiological function of primary cardiac cells; it may also be useful in electrophysiologically maturing induced pluripotent stem cell-derived cardiomyocytes.

Received 6th March 2025,
Accepted 8th September 2025

DOI: 10.1039/d5lc00234f

rsc.li/loc

Introduction

Systems for delivering electrical stimulation to *in vitro* cell cultures represent increasingly important tools in tissue engineering, particularly for their use in mimicking the electrical microenvironment within electroactive tissues. This technique is of specific interest to the fields of cardiac, muscle, and neural tissue engineering – systems whose functionality *in vivo* depends upon action potentials and their propagation between neighboring cells. Bioreactors incorporating stimulation capabilities allow for the generation of more physiologically relevant cellular microenvironments during attempts to recapitulate electrophysiological function within tissue engineered constructs.

In vitro electrical stimulation has been extensively explored in the context of cardiac tissue engineering research. In 2013, Hsiao *et al.* seeded neonatal rat cardiomyocytes (NRCMs) onto conductive scaffolds and applied electrical pacing, finding that this stimulation synchronized beating between neighboring cell clusters by facilitating gap junctional coupling.[1] Also in 2013, Kim *et al.* found that electrical stimulation of murine cardiac stem cells improved their survivability under oxidative stress.[2] Furthermore, electrical stimulation of murine cardiac stem cells restored contractility following ischemic damage in mice when transplanted into infarcted myocardium. Similarly, Serena *et al.* found that electrical stimulation contributed to cardiogenesis in human embryonic stem cells, suggesting this stimulation plays an important role in the differentiation of cardiac tissue.[3] More recently, it has been shown that electrical stimulation improves electrophysiological function in a human induced pluripotent stem cell-derived cardiomyocyte (hiPSC-CM) heart-on-chip model using hydrogel electrodes,[4] promotes membrane remodeling and enhances transverse tubule network formation in hiPSC-CMs,[5] and allows for regulation

[a] *Department of Textile Chemistry, Engineering, and Science, North Carolina State University, USA. E-mail: jmgluck@ncsu.edu*
[b] *Lampe Joint Department of Biomedical Engineering, North Carolina State University and University of North Carolina Chapel Hill, USA*
[c] *Department of Molecular Biomedical Sciences, North Carolina State University, USA*
[d] *Department of Pharmaceutical Sciences, Texas A&M University, USA*
[e] *Department of Biomedical Engineering, Columbia University, USA*
[f] *Department of Electrical and Computer Engineering, North Carolina State University, USA*
† Co-first authors with equal contributions.

of the beating rate of NRCMs *in vitro*.[6] From these and other studies, it is apparent that electrical stimulation (in the context of both stem cells and primary cells) is a powerful tool for promoting electrophysiological function and driving specific phenotypes *in vitro*.

In vitro electrical stimulation also has significance in neural tissue engineering and is a technique that has been leveraged over several decades of prior research. As early as 1979, it was shown in an embryonic chick model that neurites grow preferentially towards negatively-polarized electrodes.[7] In 1981, a frog model was used to demonstrate that the quantity of neurons generating neurites increased in the presence of an applied electrical field.[8] These and other contemporaneous studies led to the conclusion that exogenous electrical fields powerfully influence not only neurons, but also skeletal muscle cells, smooth muscle cells, neural crest cells, fibroblasts, and epithelial cells.[9] More recent studies have corroborated and expanded upon these earlier results. For example, it has been shown that electrical stimulation significantly increases (by up to 10-fold in one study[10]) and guides neurite outgrowth,[11] which is likely to prove useful for therapies targeting nerve injury by inducing neurite regeneration.[12] Additionally, the utility of electrical stimulation has been shown in the areas of bone tissue engineering,[13,14] muscle and neuromuscular tissue engineering applications,[15,16] and wound healing.[17–21]

In order to harness the power of electrical stimulation for tissue engineering applications, we aimed to develop a bioreactor system capable of electrically stimulating cells *in vitro* in a straightforward and user-friendly manner, while maintaining aseptic conditions and sterility. Current bioreactors are sufficient for electrically stimulating cells *in vitro* but lack the cost-effectiveness and ease of use of the hardware presented in this work. Many prior bioreactors, such as the ones demonstrated by Hsiao *et al.* in 2013,[1] and later by Ott *et al.*[22] and Gabetti *et al.*[23] in 2023, focus on individual custom-fabricated culture vessels, which limits throughput and requires the use of an external stimulus generator to form a complete functional unit.[1] Other bioreactors, such as the system developed by Liu *et al.*,[6] overcome this limitation by creating a multi-well stimulation platform in which multiple independent cultures can be maintained simultaneously. Additionally, the bioreactor described by Liu *et al.* represents a more complete solution due to the addition of multiple stimulus generation subsystems, which are located on a separate printed circuit board from the culture wells. In spite of these advantages, such a solution also requires complex fabrication steps (including sputtering to generate the stimulation electrodes, and assembly of the culture vessels themselves) and substantial user skill in order to effectively operate the device.

Commercial bioreactor systems are also available for electrical stimulation of cells *in vitro*, and in some cases include features such as the ability to record contractility or provide mechanical stimulation in conjunction with a standard 12-well plate. However, these systems are comparatively expensive, ranging from $17 000 (Culture Pacing System, IonOptix) to $265 000 (Mantarray, Curi Bio) depending on the combination of stimulation equipment and analysis software purchased. These systems utilize bulky, expensive, non-removable electrodes which must be cleaned between experiments (rather than simply replaced) and reduce the size of the homogeneous region of the electric field, thereby reducing the effective culture area for consistent cell stimulation. Together, these features constrain the usefulness of these commercial systems, limiting their widespread adoption.

In contrast to systems involving fabrication of purpose-built culture wells, the system we present herein leverages existing commercially available 12-well plates, which can be cheaply acquired and easily replaced, are known to be non-cytotoxic, and are compatible with other equipment found in biology labs and biomanufacturing environments (such as plate readers and automated fluid handling systems). Therefore, our bioreactor constitutes a tool allowing stimulation of *in vitro* cultures even in the absence of specialized experience or expensive equipment. This open-source system can also be fully manufactured at a cost of less than $300, and contains thin, removable carbon electrodes that are both readily replaceable to avoid contamination and maintain a homogeneous electric field over a large fraction of the total well surface area. These features remove roadblocks previously prohibiting many labs from engaging in research exploring electrical stimulation for tissue engineering.

Here, we use biocompatible carbon paper electrodes laser cut from 1% Toray Carbon Paper (TGP-H-060, Fuel Cell Earth) which are easily sterilized, easily re-used, and easily replaced when needed due to a novel electrode affixation method. After design, fabrication, and validation of our bioreactor, we analyzed its effectiveness by electrically stimulating NRCMs *in vitro*. Following 7 consecutive days of electrical stimulation for 10 minutes each day, we assessed cell viability 3, 5, and 7 days post-stimulation (referring to the number of days after the 7th day of stimulation) to determine if our bioreactor produced apoptosis or a cytotoxic response within the NRCM cultures. Finally, on day 8 post-stimulation, we performed immunocytochemical staining and real-time quantitative polymerase chain reaction (RT-qPCR) to qualitatively analyze protein expression and quantify gene expression, respectively, for markers related to cardiomyocyte electrophysiological function and a contractile phenotype. We conclude that this bioreactor system constitutes a novel and valuable tool for harnessing electrical stimulation to differentiate and mature *in vitro* cell constructs for tissue engineering applications.

Materials and methods

NRCM and NRVF harvesting

NRCMs and neonatal rat ventricular fibroblasts (NRVFs) were harvested from Sprague-Dawley rats according to NC State

IACUC protocol 22-422.[24] Two-day-old rats were euthanized, and their ventricles were dissected and minced. Heart tissue was dissociated with trypsin (25300054, Gibco) at 4 °C overnight. Following trypsinization, tissue was submerged in collagenase for 1 minute at 37 °C, then collected into DPBS kept at 4 °C; this step was repeated 5 times. From the collected tissue, NRCMs were plated with or without NRVFs in IMDM media (12440053, Gibco) and incubated with either

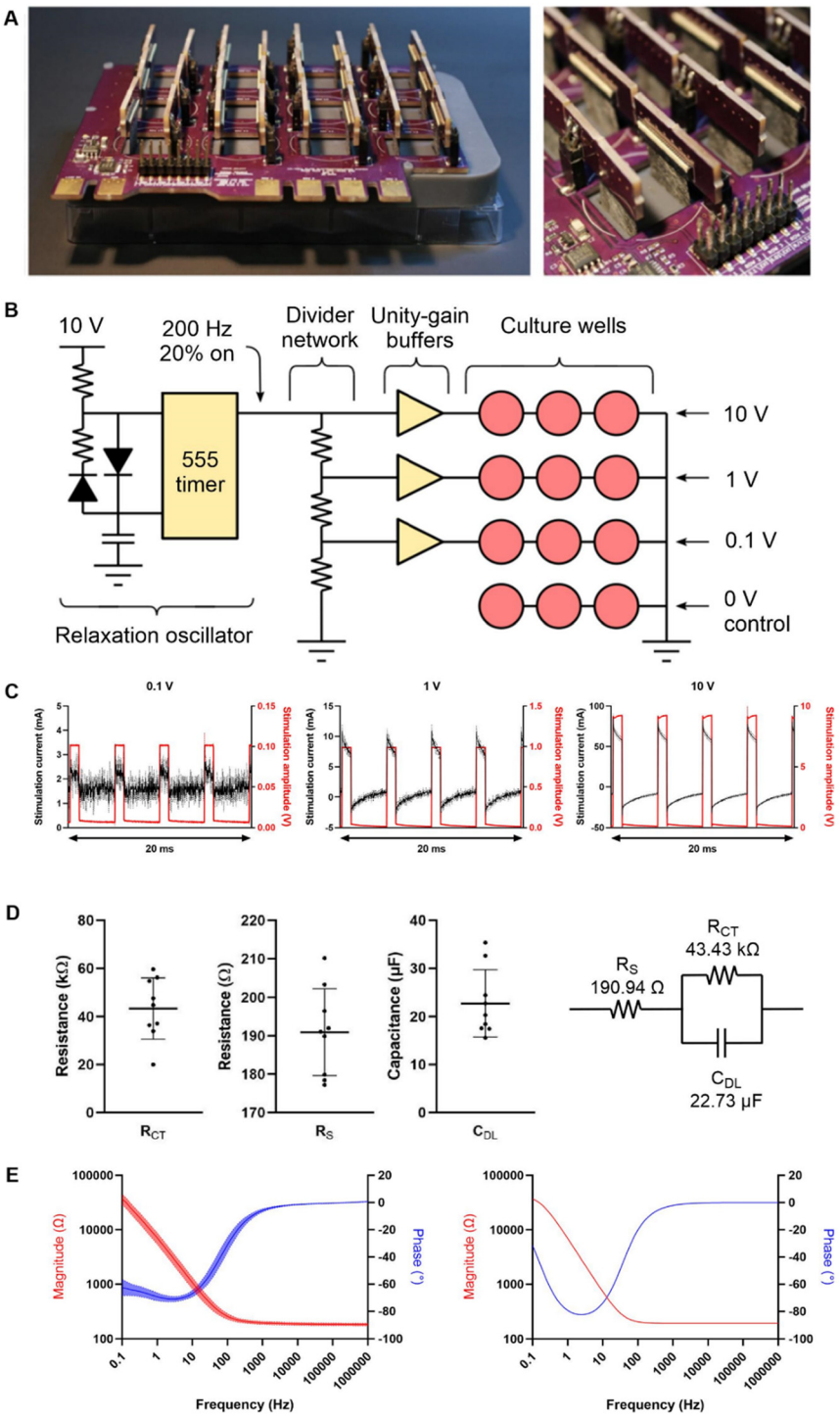

Fig. 1 Bioreactor design and characterization of electrical stimulation: A) photographs of the full bioreactor system (left) and a detail photo showing secondary PCBs attached at right angles and used to affix carbon paper electrodes within each culture well (right); B) simplified schematic of the stimulus generator circuit; C) measured stimulation voltage and current for 0.1 V, 1 V, and 10 V channels (left to right) driving individual wells containing 1 mL 1× PBS (n = 3 each, mean ± SD); D) equivalent Randles circuit component values fit from collected EIS data (n = 9, mean ± SD); E) impedance spectra of an individual well containing 1 mL 1× PBS collected using EIS (left, n = 9, mean ± SD) and reconstructed using a SPICE simulation of a Randles equivalent circuit with component values fit to EIS data (right).

10% or 2% fetal bovine serum (35-010-CV, Corning), for NRCM + NRVF co-cultures or NRCMs alone, respectively. After two hours, the NRVFs were observed to attach to the plate. The media was aspirated, centrifuged, and reconstituted with the previously described IMDM media. After cell counting, NRCMs were plated at 1×10^6 cells per cm^2 into appropriately sized flasks or well plates.

NRCM and NRVF plating and maintenance

A 12-well tissue culture plate was coated with 0.1 mg mL^{-1} human recombinant laminin 521 (LN521-05, BioLamina) diluted 1 : 1900 in PBS with calcium and magnesium and incubated overnight at 4 °C. NRCMs with and without co-cultured NRVFs were lifted from T25 flasks using 0.25% trypsin-EDTA (25200056, Gibco), centrifuged at 300*g* for 5 minutes, resuspended in IMDM supplemented with 2% fetal bovine serum for NRCMs without NRVFs, and 10% fetal bovine serum for NRCMs with NRVFs, then re-plated at equivalent passage number 2 into the laminin-coated 12-well plate. The 12-well plate was then placed in an incubator maintained at 37 °C and 5% CO_2. Beating was observed after re-plating. Media was changed daily.

Bioreactor design and fabrication

A custom bioreactor (Fig. 1) was designed to interface with a standard 12-well tissue culture plate (07-200-81, Corning). The bioreactor consisted of a primary printed circuit board (PCB) containing both the stimulus generator circuit and a set of connectors for attaching 24 secondary PCBs, and a 3D-printed interposer which replaces the lid of the 12-well plate and positions the primary PCB above the culture wells. Each of the secondary PCBs possess a connector for attaching to the primary PCB, and a second connector for inserting a laser-cut carbon paper electrode (TGP-H-060, Toray Industries). When the secondary PCBs are mounted to the primary PCB at a right angle, the carbon paper electrodes (two per well) protrude into the culture wells through narrow openings in the 3D-printed interposer. The stimulus generation circuit implements a relaxation oscillator based on a 555 timer (TLC555, Texas Instruments) to generate a fixed stimulation waveform whose frequency and duty cycle depends on the values of passive components used in the circuit. In this case, a target frequency and duty cycle of 200 Hz and 20% were selected, respectively. The resulting waveform is a unipolar square wave whose amplitude is equal to that of the system supply voltage (in this case 10 V). This signal is passed to an attenuator-buffer consisting of a precision multi-stage voltage divider and a quad-channel operational amplifier (TLV9354-Q1, Texas Instruments). Passive components in this subcircuit are selected to generate three distinct output signals of varying magnitude, in this case at 100%, 10%, and 1% of the full-scale voltage (corresponding to 10 V, 1 V, and 0.1 V, nominally); in the electrode configuration employed here, this resulted in electric field strengths of 7.24 V cm^{-1}, 0.724 V cm^{-1}, and 72.4 mV cm^{-1}, respectively. The fourth channel was not connected to the final row of culture wells to allow these to serve as an unstimulated control. Connected channels (selectable *via* an array of jumpers) pass their conditioned waveforms to each column of three wells on the 12-well plate simultaneously upon application of power to the circuit.

Stimulation characterization and finite element analysis

In order to evaluate stimulation performance, the stimulation circuit was examined through a combination of equivalent circuit simulation, simulation using a finite element analysis (FEA) model of the culture wells, and direct measurement of stimulation voltage and current. To fit an equivalent circuit model, electrochemical impedance spectroscopy (EIS) was performed on individual culture wells containing 1 mL 1× PBS (equivalent to the amount of media used during subsequent cell culture experiments) using a potentiostat (Reference 600+, Gamry). EIS was performed in a 2-electrode configuration, using the same carbon paper electrodes utilized during cell stimulation, and covering a frequency range of 0.1 Hz to 500 kHz. Resulting data were fit to a Randles equivalent circuit using the potentiostat software (Echem Analyst 2, Gamry). This equivalent circuit was then used to simulate circuit behavior in a SPICE simulation environment (LTspice, Analog Devices) in order to model current flowing through the culture well in response to the applied stimulation. SPICE simulations assumed a stimulation waveform with timing and amplitude parameters equivalent to those used for cell stimulation (200 Hz, 20% duty cycle, and 10 V, 1 V, or 0.1 V peak amplitude). Stimulus impulse rise and fall times were extrapolated from measurements taken from equivalent application of stimulus to a well containing 1 mL PBS (see Fig. S1).

FEA was performed using a 3D model of the culture well volume generated in a FEA suite (COMSOL Multiphysics 6.2, COMSOL Inc.). To model behavior of the electrode–electrolyte interface, the secondary current distribution physics interface within the COMSOL electrochemistry module was utilized. PBS electrolyte was modeled using the included water material definition, using all default values except for electrolyte conductivity which was changed to 1.6 S M^{-1}. The well volume was modeled based on the measured geometry of the culture well and the carbon paper electrodes, assuming 1 mL of electrolyte. Simulations were performed using assuming an electrode double layer capacitance equal to 28.06 μF cm^{-2}, derived from the capacitance value obtained from EIS equivalent circuit fitting (22.73 μF) and the nominal electrode surface area when 1 mL PBS is present in the well (0.81 cm^2 per electrode pair). As in the case of SPICE simulation, FEA simulation assumed a stimulation waveform with timing parameters and amplitudes equivalent to those used for cell stimulation.

The potential waveform applied to the culture wells by the stimulus generator was measured directly using an oscilloscope (Analog Discovery 2, Digilent). Stimulation

current was indirectly measured in culture wells containing 1 mL 1× PBS by measuring the resulting voltage drop across a 1 ± 0.01 ohm resistor placed in series with the culture well (*e.g.* between the stimulus generator output and the well – see Fig. S2). Except where otherwise noted, a single well was stimulated during these characterization experiments through removal of all other electrode pairs. Replicates were collected in multiple wells within each column, using multiple distinct electrode pairs to account for any possible variability between individual electrodes.

Electrical stimulation

Prior to use, the disassembled bioreactor assembly was sterilized with hydrogen peroxide, 70% ethanol, and 15 minutes of UV irradiation on each side (top and bottom) in a laminar flow hood. When electrodes broke due to material defect or user handling, which was infrequent but did occur, they were easily replaced with new Toray paper, which is inexpensive ($7.50 for a set of 24 electrodes). The bioreactor was intentionally designed to enable frequent replacement of the electrodes, if desired. Researchers using our system may elect to never re-use and re-sterilize electrodes and instead load in fresh electrodes for each experiment. After sterilization, the bioreactor was kept in a sterile environment between uses.

To perform stimulation, the bioreactor was placed onto a 12-well plate containing NRCMs, either with or without co-cultured NRVFs. 10 V DC was supplied to the bioreactor using a switch-mode bench power supply (B07X2VZSL9, NicePower), which was connected to the bioreactor using alligator clips. Upon application of power, 0.1 V, 1 V, and 10 V amplitude (nominal) stimulation waveforms were supplied to columns 2, 3, and 4, respectively, of the 12-well plate. Column 1 was reserved as an unstimulated control. Voltage was applied for 10 minutes daily at the same time each day for 7 consecutive days. No hydrogen bubbles resulting from electrolysis were observed.

Viability assays

On days 3, 5, and 7 post-stimulation, LIVE/DEAD viability assays (L3224, Invitrogen) were performed on each well (n = 6 for NRCM + NRVF, n = 3 for NRCM − NRVF) exposed to 0 V, 0.1 V, 1 V, and 10 V (nominal) stimulation. Images (n = 10) were collected using a fluorescent microscope at both 4× and 10× magnifications (EVOS FL Auto 2, Invitrogen).

On days 3, 5, and 7 post-stimulation, alamarBlue metabolic assays (n = 6 for NRCM + NRVF, n = 3 for NRCM − NRVF) were performed by adding 100 μL alamarBlue reagent (DAL1025, Invitrogen) to each well (in triplicate) of the 12-well plate containing NRCMs with and without NRVFs, in addition to 3 blank wells containing only media, and incubated at 37 °C and 5% CO_2 for 1 hour. Following incubation, 100 μL of media was taken from each well of the 12-well plate and added in triplicate to a 96-well plate. Fluorescence was quantified in arbitrary fluorescence units (RFU) using a microplate reader (Synergy HT, BioTek) set to 540/25 nm excitation and 590/35 nm emission, and maintained at 37 °C.

Immunocytochemistry and fluorescence microscopy

On day 8 post-stimulation, wells (n = 6 for NRCM + NRVF) were fixed with 4% paraformaldehyde (15735-80, Electron Microscopy Services), then permeabilized using PBS with 0.25% TritonX-100 (112298, Millipore Sigma) and PBS with 0.1% Tween-20 (BP337-100, Thermo Fisher) and serum-blocked using blocking buffer composed of PBS with 0.1% Tween-20 and 2% bovine serum albumin (BP9706100, Thermo Fisher) and 2% goat serum (16-210-064, Gibco, Thermo Fisher). Samples were incubated at room temperature in blocking buffer with primary antibodies for α-actinin (MA1-22863, Invitrogen) and connexin-43 (71-0700, Invitrogen), both diluted 1 : 250, then washed in PBS + 0.1% Tween-20. Next, samples were incubated at room temperature in PBS with 10% blocking buffer and secondary antibodies – goat anti-mouse IgG1, fluorophore 594, (A21125, Invitrogen) and goat anti-rabbit IgG (H + L), fluorophore 488 (A11008, Invitrogen) – then washed again in PBS with 0.1% Tween-20. Washed samples were counterstained with 1 : 1000 Hoechst 33342 (62249, Thermo Fisher) in PBS, re-washed in PBS, and imaged using a fluorescent microscope (EVOS FL Auto 2 Cell Imaging System, Thermo Fisher).

ImageJ was used on immunostaining images to quantify fluorescence by first separating images by red, blue, and green color channels as corresponding grayscale images. The "measure" tool was then used to quantify mean gray value within a region of interest (ROI) containing the cells, which corresponded to mean fluorescence value for this ROI.

Genetic expression analysis (RT-qPCR)

On day 8 post-stimulation, separate wells (n = 18 for NRCM + NRVF) were washed with PBS and lysed with 350 μL of Buffer RL (from Total RNA Purification kit, 17200, Norgen Biotek) for 5 minutes, then collected into microcentrifuge tubes with 200 μL of 100% ethanol. RNA was purified using the Norgen Biotek Total RNA Purification kit according to the provided protocol, in which samples were bound to spin columns placed in collection tubes, which were then washed and eluted using a benchtop microcentrifuge (Centrifuge 5415 D, Eppendorf). Eluted RNA was then evaluated for concentration and purity using a microvolume spectrophotometer (NanoDrop One, Thermo Fisher Scientific). cDNA was synthesized from the resultant RNA using a TruScript™ First Strand cDNA Synthesis kit (54420, Norgen Biotek), with RNA quantities normalized to the lowest measured RNA concentration among samples in order to ensure cDNA quantities were equal between samples. cDNA synthesis was performed using a thermocycler (Mini Amp, Applied Biosystems, Thermo Fisher Scientific) set to generate cDNA templates which were then analyzed using RT-qPCR on a quantitative PCR machine (QuantStudio 3, Applied

Table 1 Primer sequences used for qPCR

Species	Primer	Forward sequence	Reverse sequence
Rat	*GAPDH*	TCTCTGCTCCTCCCTGTTCTA	ATGAAGGGGTCGTTGATGGC
Rat	*βMYC*	TCGCACCTGGACTACAATA	TACAGGTGCATCAGCTCCAG
Rat	*cTnT*	GCCAGAGATGCTGAAGATGGT	GCACCAAGTTGGGCATGAAG
Rat	*cTnI*	CTCTGATGCTGCAGATTGCG	CTGCCGGCATAGGTCCTGAA
Rat	*GJA1 (Cx43)*	CGCCGGCTTCACTTTCATTA	CGCCGGCTTCACTTTCATTA
Rat	*Cav1*	GAGTCTGCCAAAGCAAGATTGCCA	AGGCTTCGCAGCGTTACAGACTAT

Biosystems, Thermo Fisher Scientific) running comparative cycle threshold analysis. Custom primers were acquired from Integrated DNA Technologies using the sequences shown in Table 1. Prior works were utilized to identify sequences for the following: *GAPDH*, *CX43* (also referred to as *GJA1*), *cTnI*, *cTnT*, and *βMYC* (Vaez *et al.*, 2018 (ref. 25)); and *Cav1* (Zhang *et al.*, 2012 (ref. 26)). Resultant mean cycle threshold (CT) values were analyzed using the $2^{-\Delta\Delta CT}$ method with *GAPDH* as the housekeeping gene.

Animal use

All animal procedures were performed in accordance with the North Carolina State University IACUC guidelines and were approved under IACUC protocol 22-422.

Results

Bioreactor assembly and stimulation characterization

Our bioreactor system features a simple, economical, and miniaturized on-board stimulus generator which requires only the application of external DC power to produce a unipolar voltage-controlled stimulation waveform. From this DC supply, the stimulus generator produces a full-scale square wave whose duty cycle and frequency can be easily varied through the selection of different passive components. A second stage attenuates and buffers this master signal to produce up to four distinct output voltage levels (in this case, 100%, 10%, 1%, and 0% of the full-scale voltage), each of which is simultaneously applied to three culture wells in parallel. As with the stimulus timing characteristics, these attenuation levels can also be easily varied through the selection of different passive components. Our system improves the compatibility of bioreactor-based differentiation with aseptic technique due to a minimization of the number of connectors required to operate the system within an incubator and enables the possibility of efficient scale-up as many culture vessels can be operated in parallel, without the need for a large number of costly external stimulus generators, and without utilization of time-consuming fabrication techniques.

Stimulation voltage and current were measured for all output channels to verify that an appropriate stimulus was being applied to the culture wells (Fig. 1C). On each channel, a single well was connected, and the voltage delivered to the well was recorded using an oscilloscope. Simultaneously, the voltage drop across a small shunt resistance was used to transduce delivered current, without substantially affecting the stimulation waveform (Fig. S2). In the case of the 0.1 V and 1 V channels, the nominal voltage was achieved, and a time-varying current consistent with the charging of the double layer capacitance in a Randles circuit was observed. The 10 V channel demonstrated a similar current waveform, however the applied voltage experienced a slight distortion due to loading effects, causing the output voltage of the corresponding operational amplifier channel to drop, particularly at the beginning of each stimulus pulse when the capacitive current was greatest (Fig. S3). Nevertheless, the stimulation voltage on the 10 V channel consistently remained above 8 V, even when all three wells were stimulated simultaneously (representing at least an 8-fold increase compared to the next-highest amplitude channel, accompanied by a corresponding increase in delivered current).

Simulation of cell stimulation using EIS-derived equivalent circuit model and FEA

Collected EIS data were fit to a Randles equivalent circuit, a circuit commonly used to model the electrode–electrolyte interface formed from the insertion of an electrode into a conductive solution (Fig. 1C). From these results, component values were fit to generate impedance spectra closely matching the spectra observed during EIS, ensuring that the Randles circuit demonstrates a similar frequency-dependent response to the actual electrode–electrolyte interface present during cell stimulation (Fig. 1E). Fit data obtained from EIS were used to generate a SPICE simulation of the equivalent circuit, which revealed a steady state current magnitude and transient response quite similar to those observed by direct measurement of the stimulation waveform (Fig. 2C).

FEA simulation of the stimulated culture wells was used to validate SPICE simulation data, and to provide a view of the potential gradient and current distribution present in the well during stimulation (Fig. 2A). These simulation results produced equivalent steady state and transient behavior to the simulated SPICE model of the equivalent Randles circuit for the cell (Fig. 2B and C). This FEA model predicts currents which are similar in magnitude to both those observed through direct measurement of the stimulation output as well as those modeled from EIS data. Additionally, the applied potential gradient and current distribution were found to be largely homogeneous in the area of the culture well between the two electrodes, which comprises a majority

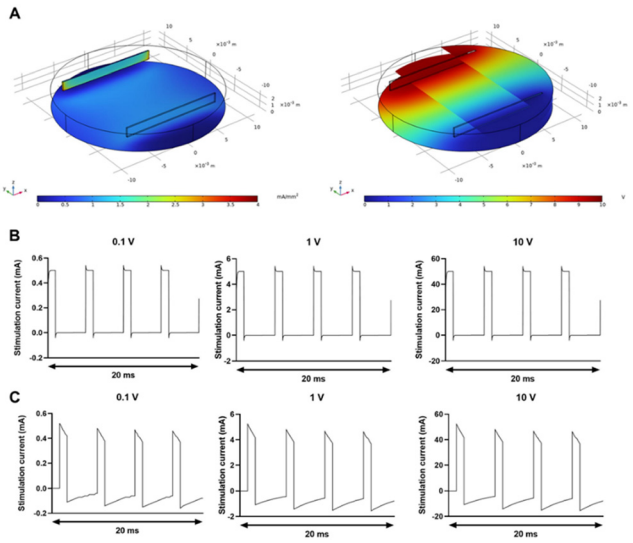

Fig. 2 FEA simulations performed in COMSOL showing A) current density (left) and potential gradients (right) developed within the culture well volume in response to the application of a 10 V stimulus; B) the resulting stimulation current observed upon application of 0.1 V, 1 V, and 10 V stimulation waveforms. FEA simulations assume 1 mL electrolyte volume (based on the amount of culture media utilized during cell culture experiments), an electrolyte conductivity of 1.6 S m^{-1}, 0.81 cm^2 surface area per electrode pair (nominal), a distance of 12 mm between electrodes, and an electrode double layer capacitance of 28.06 μF cm^{-2}; C) SPICE simulation generated from EIS data.

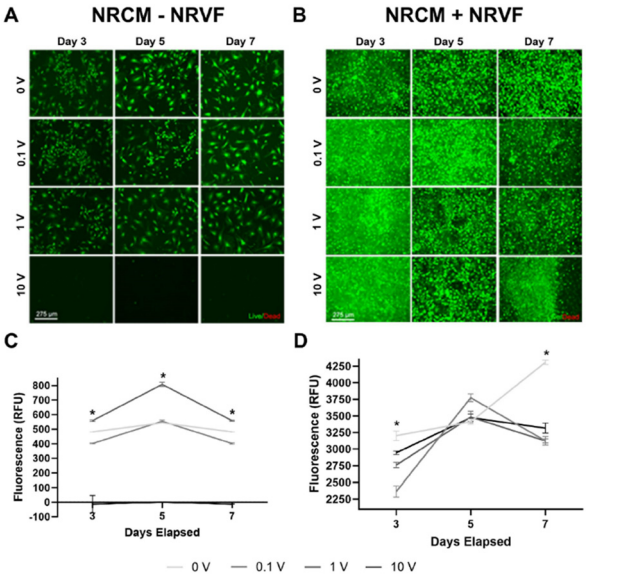

Fig. 3 Post-stimulation viability of NRCMs with and without NRVF co-culture; A and B) live/dead assay results on days 3, 5, and 7 post-stimulation; C and D) metabolic activity in arbitrary fluorescence units days 1, 3, 5, and 7 post-stimulation; * denotes statistical significance ($p < 0.05$) between groups as determined by ANOVA.

of the surface area to which cells are attached during culture. During 10 V stimulation, simulated peak current density was observed to be 1.013 mA mm^{-2} at the geometric center of the culture area, reaching a maximum value of 1.039 mA mm^{-2} at a focal point in front of each electrode. Delivered current was found to decrease significantly in the area "behind" each of the carbon paper electrodes. Importantly, the homogeneous potential gradient observed in the central portion of the well extended the full vertical height of the electrolyte, including the base of the well where the cells are located. Simulated peak power dissipation was observed to be 0.643 mW mm^{-3} at the geometric center of the culture area, and 0.675 mW mm^{-3} at the focal maxima.

Viability studies indicate high post-stimulation cell viability, except for NRCMs without NRVF post-10 V stimulation

Live/dead analyses performed on NRCMs cultured without NRVFs on days 3, 5, and 7 post-stimulation (Fig. 3A) revealed similar cellular responses for groups exposed to 0.1 V and 1 V stimulation, as well as unstimulated controls. These cells maintained their confluency and did not exhibit widespread cell death, as evidenced by the presence of green staining (indicating active cell metabolism by way of esterase activity) and healthy morphology across all three groups at all three timepoints (Fig. 3B). NRCMs cultured without NRVFs that were exposed to 10 V stimulation failed to maintain confluency, as shown by the lack of green fluorescence (Fig. 3A). The absence of red fluorescence (which would normally mark dead cells) is due to the dead cells being aspirated alongside media after detachment from the laminin coating due to compromise of their nuclear membrane following apoptosis. This is corroborated by the near-zero value of arbitrary units of fluorescence (RFU) for days 3, 5, and 7, signifying negligible metabolic activity. Clearly, 10 V stimulation is fatal to NRCMs cultured without NRVFs.

In contrast, live/dead analyses performed on NRCMs co-cultured with NRVFs on days 3, 5, and 7 post-stimulation (Fig. 3B) revealed high viability and no cytotoxicity across all four groups, including cells which underwent 10 V stimulation. For all groups, the presence of cells, maintenance of confluency over multiple timepoints, and green fluorescence indicating living cells signifies that the electrical stimulation of NRCMs with NRVFs is not actively harmful. Notably, NRVFs appear to exert a protective effect on NRCMs in co-culture, allowing them to survive 10 V electrical stimulation, which was otherwise fatal to these cells (Fig. 3A).

Further viability testing consisted of alamarBlue assays, which are used to quantify the metabolic activity of cells. NRCMs without NRVFs subject to 10 V stimulation (Fig. 3C) exhibited virtually no metabolic activity at all timepoints, indicating the absence of living cells and corroborating the corresponding live/dead assay results (Fig. 2A). NRCMs without NRVFs subject to 0.1 V and 1 V stimulation, as well as the unstimulated controls (Fig. 3C) exhibited significantly more metabolic activity than NRCMs without NRVFs subjected to 10 V stimulation on days 3, 5, and 7. alamarBlue assays performed on NRCMs with NRVFs (Fig. 3D) revealed significant differences in metabolic activity between 0 V, 0.1 V, 1 V, and 10 V stimulated groups on day 3 but not day 5, indicating that though some initial differences in cell

quantity and/or metabolic activity may exist in response to varying magnitudes of stimulation, they do not persist beyond day 5 with the exception of the 0 V control expressing a significantly higher level of metabolic activity on day 7. It is important to note that metabolic activity assay results cannot be directly compared between NRCMs with and without NRVFs in co-culture. alamarBlue assays measure fluorescence exhibited by resorufin, which is produced when non-fluorescent resazurin is reduced by the metabolic activity of living cells, normalized to a blank control containing only media. Because trials with and without NRVFs were run at different times, comparisons between measured RFU values are relevant only between groups of each trial; differences between trials cannot be analyzed using this method.

Immunostaining reveals favorable response to 0.1 and 1 V stimulation and adverse response to 10 V stimulation

Due to the superior response of NRCMs co-cultured with NRVFs to electrical stimulation as shown in viability studies

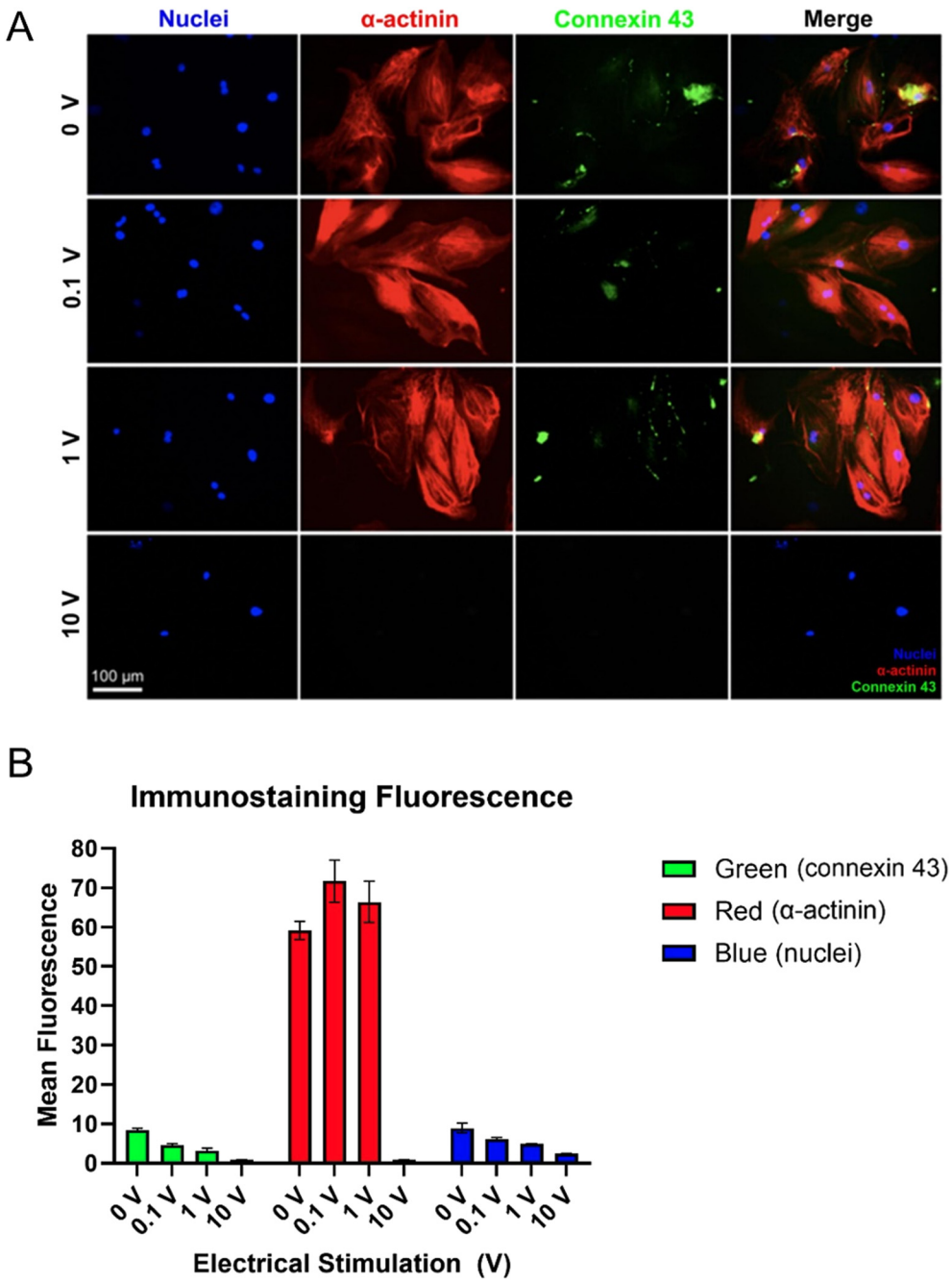

Fig. 4 (A) Immunofluorescent staining for expression of nuclei (blue), sarcomeric α-actinin (red), and connexin 43 (green) on day 8 post-stimulation for NRCMs co-cultured with NRVFs. Images taken at 10×. (B) Mean fluorescence quantification performed on ImageJ for red, blue, and green fluorescence within immunostaining image.

(Fig. 3), we conducted the remaining experiments using NRCMs co-cultured with NRVFs. NRCM–NRVF co-cultures were fixed on day 8 post-stimulation and immunostaining was performed (Fig. 4). We selected two markers associated with a cardiomyocyte-like phenotype: sarcomeric α-actinin (stained red), to analyze cellular mechanisms associated with contractility within NRCMs, and connexin 43 (Cx43, stained green) to assess the presence of gap junctional coupling between neighboring NRCMs, thereby signifying their ability to form a syncytium similar to that encountered *in vivo* and propagate action potentials between adjoining cells. We also stained nuclei blue (DAPI). Similar results were observed for both the unstimulated control and the 0.1 V stimulation groups, wherein α-actinin was expressed prominently and with the appropriate striated morphology necessary for interaction with myosin filaments to generate cellular contraction. Connexin 43 was also expressed with appropriate localization between neighboring cardiomyocytes, where it serves to provide a low impedance electrolyte bridge between adjacent NRCMs to facilitate electrical coupling. Connexin 43 was expressed highest in the unstimulated control (mean gray value 9.75), then 0.1 V (mean gray value 4.391), then 1 V (mean grey value 3.198), and least in 10 V stimulated NRCM (mean gray value 0.91) (Fig. 4B). NRCMs co-cultured with NRVFs exposed to 1 V stimulation demonstrated both increased expression of α-actinin (Fig. 4B) and increased striation within α-actinin (Fig. 4A) compared to 0.1 V and 10 V stimulation groups and unstimulated controls, suggesting superior contractile physiology. NRCMs co-cultured with NRVFs exposed to both 0.1 and 1 V stimulation also exhibited increased expression (Fig. 4B) and appropriate localization (Fig. 4A) of connexin 43 compared to the non-stimulated control, indicating an increased quantity of formed gap junctions, suggesting improved inter-cell electrical coupling. NRCMs co-cultured with NRVFs exposed to 10 V stimulation expressed negligible α-actinin and connexin 43 (Fig. 4A and B), and DAPI staining indicated the presence of nuclei (Fig. 4A and B), but less visibly expressed within the unstimulated control and the 0.1 V and 1 V stimulation groups. Overall, we conclude that with regards to expression of α-actinin and connexin 43 on day 8 post-stimulation, NRCMs co-cultured with NRVFs responded most favorably to 0.1 V stimulation, then 1 V stimulation, and negatively to 10 V stimulation.

RT-qPCR reveals overall upregulation post-0.1 V stimulation and overall downregulation post-10 V stimulation

We used the $2^{-\Delta\Delta CT}$ method to analyze RT-qPCR data in order to quantify the genetic expression of *βMYC* (β myosin heavy chain), *cTnT* (cardiac troponin T), *cTnI* (cardiac troponin I), *Cx43*/*GJA1* (connexin 43), and *Cav1* (caveolin 1) in NRCMs co-cultured with NRVFs. β myosin heavy chain, cardiac troponin T, and cardiac troponin I are indicative of a functional contractile phenotype. β myosin is expressed within myosin filaments partially responsible for contractile force upon depolarization. Cardiac troponins T and I are part of the troponin complex involved in the crossbridge cycling mechanism within cardiomyocytes which controls contraction in response to calcium transients. Connexin 43, as previously discussed, is one of the 21 proteins present in cardiac gap junctions. Finally, caveolin 1 is associated with formulation of caveolae,[27] which are partially responsible for the calcium handling necessary for excitation–contraction coupling in cardiomyocytes. Together, these genes constitute a comprehensive sampling of gene expression pertinent to the electrical and contractile phenotypes observed in typical cardiomyocyte physiology.

RT-qPCR results (Fig. 5) indicated upregulation of genes associated with cardiac electrophysiology (except *cTnT*) in NRCMs co-cultured with NRVFs exposed to 0.1 V stimulation within our bioreactor. In order of decreasing magnitude, upregulated genes were *cTnI* (14.88), *βMYC* (8.51), *Cx43* (6.92), and *Cav1* (6.92). *cTnT* was the only gene downregulated in response to 0.1 V stimulation. In response to 1 V stimulation, cardiac genes expressed slight upregulation, notably less drastic than the upregulation due to 0.1 V stimulation, except *Cav1*, which was upregulated by 2.27 gene-fold expression in response to 1 V stimulation and 0.31 in response to 0.1 V stimulation. In order of decreasing magnitude, the genes upregulated in response to 1 V electrical stimulation were *Cav1* (2.27), *βMYC* (2.17), *cTnT* (0.06), *cTnI* (3.76×10^{-4}), and *Cx43* (1.97×10^{-6}). All genes were downregulated in response to 10 V stimulation except *cTnI* and *Cx43*, both of which were only negligibly

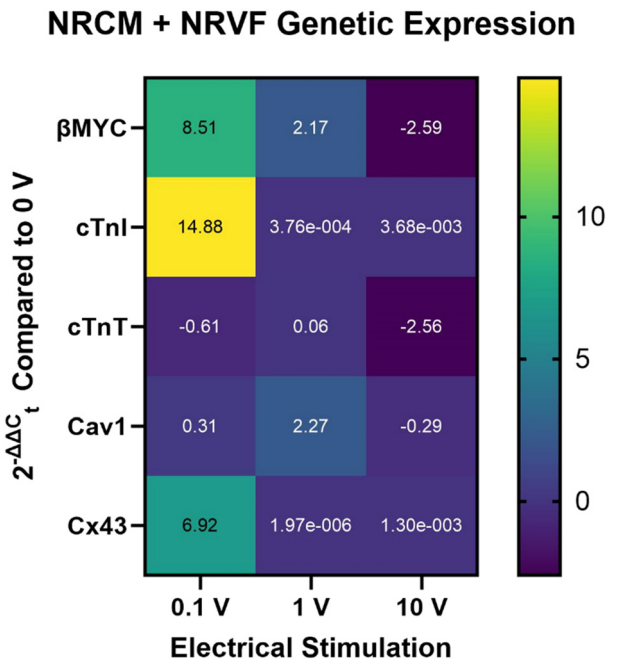

Fig. 5 RT-qPCR quantification using the $2^{-\Delta\Delta CT}$ method for genes βMYC encoding β myosin heavy chain, cTnI encoding cardiac troponin I, cTnT encoding cardiac troponin T, Cav1 encoding caveolin 1, and Cx43/GJA1 encoding connexin 43 as expressed in NRCM with NRVF co-culture at day 8 post-stimulation.

upregulated (3.68×10^{-3} and 1.30×10^{-3}, respectively). In order of decreasing magnitude, the genes downregulated in response to 10 V stimulation were *βMYC* (−2.59), *cTnT* (−2.56), and *Cav1* (−0.29).

Discussion

Measurement of the applied stimulation waveform (including both direct measurement of stimulation voltage and indirect, shunt-based measurement of the delivered current) revealed that the bioreactor stimulation circuit adheres to the intended design goals. Notably, the 10 V stimulation channel is susceptible to loading effects which drive the actual delivered voltage to a lower value than the nominal stimulation voltage. This is particularly true when multiple wells are stimulated with the same 10 V output simultaneously. While this is a relatively minor limitation, the possibility of overloading the other output channels – *e.g.* through the introduction of a larger number of parallel wells, or a greater volume of culture media – makes this limitation a high priority to address in future versions of the system. Remedies for this issue include the use of higher output current operational amplifiers, or through the incorporation of a transistor-based gain stage into the operational amplifier output circuit, in order to boost the current driving capability of each output channel.

During use, practical experience with the fabricated bioreactor hardware supported our choice to use a modular electrode-holding system, as this allowed for rapid and easy replacement of the carbon paper electrodes in the event that individual electrodes were damaged or contaminated. The carbon paper selected for this role proved sufficiently stable for use in protracted stimulation experiments. No visible degradation to the carbon paper electrodes used in this experiment was observed, excluding damage during insertion which occasionally occurred. Nevertheless, the combination of carbon paper electrodes and a connector-based mounting system appears to represent a cost-effective method for delivering electrical stimulation to an array of culture wells.

In order to better understand and characterize the behavior of the stimulation circuit, and to examine the effect of stimulation on the wells themselves, two methods of simulation were employed: first, SPICE simulation allowed for the validation of the extracted Randles circuit through reproduction of the impedance spectra collected using EIS, and allowed for arbitrary stimulation and load conditions to be simulated together prior to making changes to the system; second, FEA modeling (validated in turn by SPICE simulations) enabled the spatial characteristics of a stimulation pulse to be modeled. This step was critical to ensuring that the target cells, which exclusively reside on the floor of the culture wells, were receiving sufficient stimulation during these experiments. SPICE and FEA simulation results closely followed ground truth data, indicating that these simulations are largely reliable for use as predictive design and validation tools. Stimulation current was observed to extend in a homogeneous fashion to most of the floor surface of the targeted culture wells. Only a small "shadow" exists in which stimulation current is dramatically lower, and this is not expected to limit the usefulness of the stimulation circuit.

We selected 0.1, 1, and 10 V magnitudes for NRCM experiments to reflect the range of voltages clinically used for pacemaking and myocardial capture. Typically, these voltages range from 1–5 V and 0.5–5 V, respectively.[28] Notably, these ranges vary based on clinical considerations such as medications, electrolyte imbalances, metabolic factors, specific heart conditions, device settings (*e.g.* lead position, electrode size, pacing mode), and patient-specific factors.[29] Importantly, these ranges are chamber-specific. Voltages are slightly higher for atrial pacing because atrial walls are thinner than ventricular ones, affecting electrical conduction. According to guidelines from the American College of Cardiology and American Heart Association, the maximum value for reasonable use in myocardial capture is 10 V;[30] thus, we set our highest voltage level at 10 V. Because our system applies electrical stimulation to monolayer *in vitro* cultures rather than intact *in vivo* tissues, we chose a magnitude of 0.1 V as the lower limit of our tested range. The peak voltages applied by our bioreactor are thus informed by clinical guidelines relevant to pacing and myocardial capture, in hopes that our *in vitro* stimulation affects cardiac cells in a similar fashion to existing clinical interventions.

The majority of experiments involving stimulation of cardiomyocytes *in vitro* involve stimulation frequencies similar to those employed in pacing of cardiac cells *in vivo*, typically in the range of 1 Hz to 5 Hz (with slightly higher frequencies utilized in the case of rat cells due to their higher resting heart rate). This is explained by the fact that these stimulation experiments attempt to recapitulate normal cardiac electrophysiology. However, physiologically-relevant changes have been observed at higher stimulation frequencies, as well, including changes in the expression of growth factors[31] which may be beneficial to the development of cardiomyocyte-like phenotypes. Our results additionally support the possible efficacy of this higher-frequency approach, however additional work is needed to further explore this stimulation regime, particularly in the areas of supra-threshold (*i.e.*, capable of directly evoking action potentials and contractility) electrical stimulation, and combined high-/low-frequency and sub-/supra-threshold stimulation protocols. Importantly, our bioreactor is well-suited for both high-frequency stimulation and conventional pacing, and is able to cover the full range of these frequencies of interest through substitution of a handful of passive components.

It is probable that some radical formation occurs within cell culture media during stimulation at elevated potentials, particularly during 10 V stimulation, and this is very likely at least a partial explanation for the reduction in cell viability observed in NRCM-only cultures stimulated at this

amplitude. However, as observed with the NRCM + NRVF co-cultures, if this radical formation occurs in sufficient quantities to potentially affect viability, this appears to be dependent on specific culture parameters (indeed this may be at least a partial explanation of the apparent protective effect conferred by NRVFs). At lower stimulation potentials (1 V and especially 0.1 V), production of radical species is expected to be dramatically decreased or eliminated entirely: oxidation of water to hydrogen peroxide, for example, typically requires an overpotential of 1 V to 1.2 V or even higher, depending on the electrode material in question; it is not certain that this reaction will occur during 1 V stimulation, and is prohibited at 0.1 V stimulation. Potentials of up to 1 V (and beyond) are routinely employed in electrochemical biosensors (and impedimetric sensing) *in vivo* and in culture without apparent ill effect, and this is further supported by the results of our viability experiments. Further, the presented data suggest that (for this cell line and other stimulation parameters) the optimal stimulation amplitude is less than 1 V. However, it is important to note that the excessive accumulation of reactive oxygen species is known to reprogram cardiomyocyte gene function *via* transcription factors such as Nrf2 (ref. 32) and NF-κB.[33] We recommend experiments quantifying their expression following stimulation. If such experiments prove concerns regarding detrimental reactive species generation credible, this could be mitigated in culture through dilution in a larger volume of liquid media, active scrubbing of the media, and/or more frequent media changes, as appropriate to the culture/differentiation protocols being used with the cell line in question.

We conclude from viability studies (Fig. 3) that our custom bioreactor exhibits a high degree of cytocompatibility. Immunostaining (Fig. 4) revealed that NRCMs with NRVFs exposed to 10 V stimulation retained living cells (Fig. 3B) and expression of nuclei (Fig. 4) while NRCMs exposed to 10 V stimulation without NVRF co-culture did not contain any living cells (Fig. 3A). We propose three possible mechanisms to explain this difference: 1) NRVFs confer an electro-protective effect towards NRCMs allowing them to survive 10 V stimulation, albeit with a loss of function; 2) NRCMs de-differentiate to a myofibroblast-like phenotype under to 10 V stimulation; and/or 3) 10 V stimulation is cytotoxic to NRCMs but not to NRVFs.

1) NRCMs co-cultured with fibroblasts exhibited similar viability across days 3, 5, and 7 post-stimulation based on live/dead assays (Fig. 3B) and days 1, 3, 5, and 7 post-stimulation based on metabolic assays (Fig. 3D), with no significant difference between observed metabolic activities at these time points. Notably, the presence of neonatal rat ventricular fibroblasts (Fig. 3B and D) allowed NRCMs to withstand 10 V electrical stimulation, which was cytotoxic to NRCMs cultured alone (Fig. 3A and C). This suggests that the presence of fibroblasts is potentially protective towards NRCMs undergoing electrical stimulation. We hypothesize this is analogous to the widely demonstrated role of cardiac

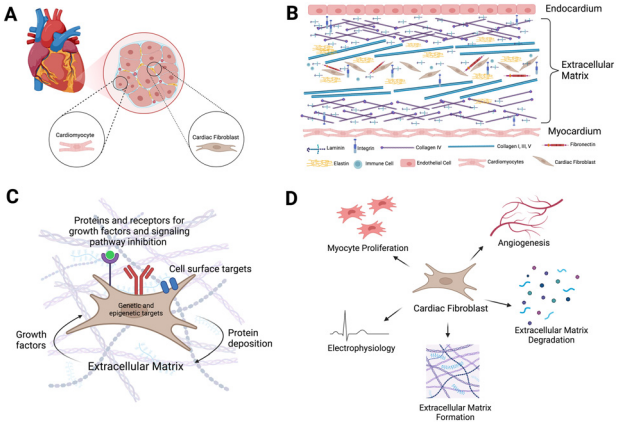

Fig. 6 Cardiac fibroblasts: A) arrangement of cardiomyocytes and cardiac fibroblasts in the myocardium; B) composition of the cardiac extracellular matrix; C) cell surface signaling, growth factor exposure, and extracellular matrix interactions influence cardiac fibroblasts; D) influence of cardiac fibroblasts on cardiovascular function.

fibroblasts *in vivo*: maintenance and regulation of heart function through the synthesis and deposition of cardiac extracellular matrix (ECM) proteins (Fig. 6C).[34–37] Cardiac fibroblasts are also known for their role in controlling ECM degradation, cardiomyocyte proliferation, cardiac electrophysiology, and cardiac angiogenesis[38] (Fig. 6D). In 2022, Bowers *et al.* proposed multiple mechanisms through which fibroblasts orchestrate cellular crosstalk in the cardiac ECM, not only through the deposition of relevant proteins, but also through communication between fibroblasts, myofibroblasts, macrophages, and cardiomyocytes mediated by the ECM itself. Specifically, fibroblasts are affected by cytokines and growth factors released by macrophages as well as tension and growth factors from the ECM, which is simultaneously created by protein deposition and influenced by growth factors from fibroblasts (Fig. 6C). Bowers *et al.* posit that cardiac fibroblasts and cardiomyocytes "sense" one another through the dynamic ECM environment; in the developmental stage, fibroblasts contribute to ECM maturation, which in turn contributes to cellular maturation within cardiomyocytes, and in disease states, myofibroblasts induce excess ECM deposition, leading to cardiomyocyte hypertrophy.[34] The role of cardiac fibroblasts is clearly pivotal for the health and functionality of cardiomyocytes *via* the maintenance of the cardiac ECM (Fig. 6C and D).

Researchers such as Fan *et al.* (2020)[39] and Kahn-Krell *et al.* (2022)[40] exploit this functional relationship between cardiac fibroblasts, cardiomyocytes, and the ECM in order to mature iPSC-CMs: Fan *et al.* used fibroblast growth factor 1 (in conjunction with CHIR 99021) to recapitulate electrophysiological function in an iPSC-CM-based cardiac patch to treat myocardial infarction, while Kahn-Krell *et al.* co-cultured iPSC-CMs with iPSC-derived fibroblasts, endothelial cells, and smooth muscle cells to develop tissue engineered cardiac spheroids. We found the relationship between fibroblast co-culture and withstanding higher

voltages interesting in this regard and deserving of further investigation. However, we note that 10 V electrical stimulation far exceeds what would normally be experienced by rat (or human) cardiomyocytes under normal circumstances *in vivo*.

2) Another possible mechanism explaining the difference in response of NRCMs cultured with *versus* without NRVFs to 10 V stimulation is the de-differentiation of NRCMs into a myofibroblast-like phenotype due to the high voltage of the applied electrical stimulation. Cardiomyocyte de-differentiation is a well-studied phenomenon involving cardiomyocyte remodeling characterized by changes in expression from mature to immature cardiac genes, disassembly of contractile physiology, and reduced cellular energy demand.[41,42] Notably, cardiomyocyte de-differentiation is defined as de-differentiation of mature adult cardiomyocytes, whereas this study uses neonatal ones. Typically, this remodeling occurs in response to ischemic injury;[43] however, we find it likely that a similar response may occur following damage due to 10 V electrical stimulation, which is far greater than any voltage that would ordinarily be encountered in the cellular environment, in either humans or rats.

3) A third mechanism possibly responsible for the difference in response of NRCMs with *vs.* without NRVFs to 10 V stimulation is cytotoxicity of 10 V stimulation to NRCMs but not to NRVFs. Thus, remaining nuclei (Fig. 4) may simply belong to NRVFs, additionally explaining why they do not express cardiac markers (Fig. 4 and 5).

Due to the aforementioned mechanisms (or possible combinations thereof), subsequent experiments investigated NRCMs co-cultured with NRVFs because they exhibit higher viability (hypothesis 1 and/or 3) and/or enhanced cardiomyocyte-like phenotype (hypothesis 2) following 10 V stimulation. Immunostaining (Fig. 4) revealed that the expression of contractile physiology and gap junctional coupling was severely diminished for NRCMs without NRVFs stimulated with 10 V; they lack the expression of α-actinin and connexin 43 expressed in the unstimulated control, as well as the 0.1 V and 1 V stimulation groups. This lack of α-actinin indicates the absence of a cardiomyocyte-like contractile phenotype, specifically with regards to sarcomeric units responsible for generating contractile force. The observed lack of connexin 43 indicates the absence of gap junctions between neighboring cardiomyocytes, which are normally responsible for the propagation of action potentials and the formation of a cardiac syncytium. The presence of healthy nuclei for the NRCM + NRVF stimulated with 10 V, though reduced, dictates that either the remaining cells are NRVFs (hypothesis 3) or myofibroblasts (hypothesis 2) and thus do not express cardiac markers, or that some NRCM survival occurred but their cardiac function was decimated, thus reducing their expression of cardiac markers.

Notably, NRCMs appeared to exhibit a preference towards 1 V electrical stimulation, as demonstrated by the superior metabolic activity of NRCMs undergoing 1 V stimulation without NRVF co-culture (Fig. 3C), as well as the increased expression of α-actinin and connexin 43 in NRCMs co-cultured with NRVFs (Fig. 4) exposed to equivalent stimulation. In a systematic review by Scott *et al.* in 2022, the authors noted in a survey of twelve publications exploring electrical stimulation of cardiomyocytes in the presence of conductive scaffolds that the most frequently used stimulation comprised of 1–3 V square pulses with 50 ms pulse width and 1 Hz frequency. This indicates that the positive response of NRCMs to 1 V stimulation is consistent with other studies, though the both the frequency and duty cycle employed in this work were substantially higher (200 Hz and 20%, respectively).[44]

Significant upregulation of *βMYC* (Fig. 5) in cardiomyocytes exposed to 0.1 V stimulation compared to non-stimulated NRCMs suggests that this magnitude of stimulation develops contractile physiology within NRCMs. Significant upregulation of *cTnI* suggests increased production of cardiac troponin I, the part of the troponin complex responsible for preventing binding to actin during relaxation. However, slight downregulation of *cTnT* suggests decreased production of cardiac troponin T, which binds to tropomyosin, thereby regulating contraction and relaxation. Though these results paint a contradictory picture of the overall response of the troponin complex to 0.1 V stimulation, the upregulation of *cTnI* is significantly greater than the downregulation of *cTnT*, suggesting the overall production of the cardiac troponin complex (consisting of troponin C, T, and I) is increased. A slight upregulation of *Cav1* suggests slightly increased T-tubule formation, which corresponds to more mature intracellular calcium handling. Significantly upregulated *Cx43* signifies increased expression of the protein associated with gap junctional coupling within cardiomyocytes, thus indicating greater development of a functional cardiac syncytium in NRCMs stimulated with 0.1 V stimulation. In response to 1 V stimulation, cardiac genes were negligibly to slightly upregulated, suggesting an overall increase in electrophysiological function, but not as significant as in response to 0.1 V stimulation. In response to 10 V electrical stimulation, cardiac genes were downregulated with the exceptions of *cTnI* (3.68×10^{-3}) and *Cx43* (1.30×10^{-3}), which were both only negligibly upregulated. Significant downregulation of *βMYC* (−2.59) and *cTnT* (−2.56) suggests a reduction in the number of myosin heavy chain and cardiac troponin T proteins, thus indicating reduced contractile physiology and impaired excitation–contraction coupling, respectively. Slight reduction of *Cav1* expression (−0.29) indicates slight impairment of T-tubule formation, thereby suggesting that calcium handling and action potential generation are both negatively impacted. qPCR results suggest that 10 V stimulation has overall negative effects on electrophysiological function of NRCMs (Fig. 5).

The limitations of our study include the limited number of timepoints analyzed (days 3, 5, and 7 post-stimulation for viability assays and day 8 post-stimulation for immunostaining and genetic analysis), re-plating of NRCMs

post-harvesting, and the assumption that our conclusions derived from an *in vitro* rat model translate to human cardiac cells.

Future steps based on the conclusions from this study include expanded applications of our bioreactor in the area of cardiac tissue engineering, potentially in combination with recent developments in cardiac patches,[45] and specifically for recapitulation of cardiomyocyte electrophysiology associated with excitation–contraction and gap-junctional coupling. We are particularly interested in the use of our bioreactor for the electrophysiological maturation of human iPSC-CMs (hiPSC-CMs). A study by Hernández *et al.* showed that electrical stimulation of embryoid bodies consisting of hiPSC-CMs led to significant upregulation of cardiac genes in one hiPSC line, but not another.[46] Two recent studies explored hydrogel models for hiPSC-CM maturation. One employed a polyvinyl alcohol hydrogel-based microchamber with carbon-based electrodes to apply electrical stimulation to hiPSC-CM spheroids.[47] The other used conductive hydrogel pillar electrodes to create a heart-on-a-chip platform in which hiPSC-CMs were electrically stimulated alongside cardiac fibroblasts.[4] Based on these and other studies, electrical stimulation represents a powerful tool for electrophysiologically maturing iPSC-CMs, but further investigation is required to fully leverage this strategy. Our bioreactor is an appropriate tool to conduct studies to explore the role of line dependency on electrical stimulation-based maturation of iPSC-CMs as well as ideal parameter selection for such techniques (*i.e.* the use of voltage- or current-controlled stimulation, stimulation amplitude, frequency, duty cycle, and duration, timing of stimulation relative to cellular differentiation stages, *etc.*). Considerations regarding differences between hiPSC-CM and NRCM culture are summarized in Table 2.

Additionally, the previously discussed electro-protective function of NRVFs when co-cultured with NRCMs represents a phenomenon worthy of additional exploration, including testing a wider range of stimulation amplitudes and using qPCR to probe the temporal progression of genetic cardiac markers following electrical stimulation at varying timepoints for varying durations. Our bioreactor has additional applications outside the area of cardiac tissue engineering. As previously mentioned, muscle, neural, and bone tissue engineering also benefit from electrical stimulation, and our bioreactor is compatible with any cell type that can be cultured on 12-well plates, which includes *in vitro* cultures of any variety of cell, at least in theory. Furthermore, our bioreactor can, in principle, be interfaced with other electrophysiological techniques (calcium- or voltage-sensitive dye, optical mapping, multielectrode arrays, patch clamping, *etc.*) to enable analysis of cardiomyocyte electrophysiology in response to electrical stimulation down to the resolution of action potentials of single cardiomyocytes and/or characteristics of gap junctions.

We plan to develop additional, improved versions of this bioreactor as part of our future efforts. First, subsequent modifications to the general circuit architecture used in this work are being pursued to allow for improved system reliability, easy reconfiguration of stimulation parameters (specifically voltage, frequency, and duty cycle) to suit a wider variety of experimental requirements, and quick visual confirmation of delivery of an appropriate level of current to the targeted culture wells. Second, a revised architecture incorporating several additional features is also being developed, in order to improve the availability of stimulation data and provide researchers with maximum flexibility as different stimulation–differentiation paradigms are pursued. Rather than employing hardware-defined stimulation parameters which are ultimately limited to voltage-controlled, two-level pulse trains, we intend for the next generation bioreactor to be capable of dynamically varying the current stimulation parameters exposed in the current bioreactor architecture (amplitude, frequency, and duty cycle) based on user-supplied commands, allowing for adjustment nearly in real-time. Additionally, features such as bipolar and current-mode stimulation, stimulation current recording, autonomous operation, and wireless control (among others) are expected to dramatically expand the possibilities afforded by our system, both to researchers studying fundamental influences of electrical stimulation on tissue, as well as in mature differentiation processes in which scale-up is required. Such a device would allow researchers to quickly examine the effects of stimulation on different populations of cells, or on the differentiation of iPSCs into distinct cell types, such as ventricular cardiomyocytes, atrial cardiomyocytes, and pacemaking cardiomyocytes. Additionally, this system could allow for the introduction of more nuanced stimulation schemes, including parameters which vary depending on feedback from observed cellular behavior. The next-generation bioreactor architecture will also feature a stimulus timing generation circuit that is substantially more immune to temperature-based variation

Table 2 NRCM and hiPSC-CM properties related to bioreactor use

Characteristic	Ventricular NRCM	Ventricular-like hiPSC-CM	Bioreactor considerations
Species	Rat	Human	None
Culture conditions	Typically DMEM, IMDM, or M199 supplemented with FBS	Differentiation protocols require different media	Minor differences in media conductivity (will not affect bioreactor, which is voltage-controlled)
Electrophysiology	Approximately −80 mV resting membrane potential with 100–200 ms action potential duration[48]	−50 to −75 mV resting membrane potential[49] with 250–500 ms action potential duration	May require tuning of voltage and frequency to optimize stimulation

than the relaxation oscillator employed here; this improvement is likely to be better suited to providing precise stimulation to cells which may be exposed to varying temperature environments during processing or over the course of an experimental protocol (*e.g.* the incubator and laminar flow hood). Together, these improvements are expected to situate our bioreactor system as a viable tool for the flexible and scalable production of engineered tissue constructs employing depolarizable cells.

Conclusions

Our bioreactor offers demonstrable advantages over previously published alternatives; namely its low cost and open source availability, ease of sterilization and use, modular design, and validation using both SPICE and FEA modeling as well as actual cellular studies using NRCMs. These *in vitro* studies using NRCMs indicated a favorable electrophysiological response to 0.1 V electrical stimulation, consistent with development of a cardiac phenotype. Further investigations of interest include electrical stimulation of hiPSC-CMs to generate electrophysiologically-mature phenotypes, fabricating a next generation of our bioreactor with upgraded capabilities, and exploring the role of NRVFs in the presence of NRCMs to 10 V stimulation. We are optimistic that our novel bioreactor is capable of facilitating these studies and proving valuable in other applications for tissue engineering and broader biomedical research endeavors.

Author contributions

SHC: conceptualization, methodology, validation, investigation, writing – original draft, visualization, formal analysis; JT: conceptualization, methodology, hardware, software, validation, investigation, writing – original draft, visualization, formal analysis; YL: investigation; KMA: investigation; DZ: investigation; KG: investigation; LM: investigation, writing – original draft; KH: supervision, resources, funding acquisition; KC: supervision, resources, funding acquisition; MAD: supervision, resources, funding acquisition, writing – review & editing; JMG: conceptualization, supervision, resources, funding acquisition, writing – review & editing. Suh Hee Cook and Jack Twiddy are co-first authors and contributed equally.

Conflicts of interest

There are no conflicts to declare.

Data availability

Supplementary information is available. See DOI: **https://doi.org/10.1039/D5LC00234F**.

Data from this article, including SPICE, FEA, cell viability, immunostaining, and RT-qPCR datasets, as well as the SI figures, are available on scienceDB at **https://doi.org/10.57760/sciencedb.21337**.

Acknowledgements

American Heart Association – CDA 942125 (JMG), Wilson College of Textiles at North Carolina State University (SHC, JMG), Provosts' Fellowship at North Carolina State University (SHC), American Association of Textile Chemists and Colorists (SHC), North Carolina State University Research and Innovation Seed Funding (JMG, MAD, SHC). Additional acknowledgements: Wilson College of Textiles, North Carolina State University, Raleigh, NC, USA; College of Veterinary Medicine, North Carolina State University, Raleigh, NC, USA; Lampe Joint Department of Biomedical Engineering, North Carolina State University, Raleigh, NC, USA and University of North Carolina Chapel Hill, Chapel Hill, NC, USA; Chemistry and Microscopy Laboratory, Textile Engineering, Chemistry, and Science, Wilson College of Textiles, North Carolina State University, Raleigh, NC, USA; Physical Testing Laboratory, Zeiss Textiles Extension, North Carolina State University, Raleigh, NC, USA; and Histology Research Core, the University of North Carolina at Chapel Hill, NC, USA.

Notes and references

1 C.-W. Hsiao, *et al.*, Electrical coupling of isolated cardiomyocyte clusters grown on aligned conductive nanofibrous meshes for their synchronized beating, *Biomaterials*, 2013, **34**, 1063–1072.
2 S. W. Kim, *et al.*, Cardiac stem cells with electrical stimulation improve ischaemic heart function through regulation of connective tissue growth factor and miR-378, *Cardiovasc. Res.*, 2013, **100**, 241–251.
3 E. Serena, *et al.*, Electrical stimulation of human embryonic stem cells: Cardiac differentiation and the generation of reactive oxygen species, *Exp. Cell Res.*, 2009, **315**, 3611–3619.
4 F. Zhang, *et al.*, Continuous contractile force and electrical signal recordings of 3D cardiac tissue utilizing conductive hydrogel pillars on a chip, *Mater. Today Bio*, 2023, **20**, 100626.
5 A. Sesena-Rubfiaro, *et al.*, Membrane Remodeling of Human-Engineered Cardiac Tissue by Chronic Electric Stimulation, *ACS Biomater. Sci. Eng.*, 2023, **9**, 1644–1655.
6 J. Liu, *et al.*, High-throughput rhythmic regulation of cardiomyocytes by integrated electrical stimulation and video-based automated analysis biosensing platform, *Biosens. Bioelectron.*, 2022, **209**, 114252.
7 L. F. Jaffe and M. Poo, Neurites grow faster towards the cathode than the anode in a steady field, *J. Exp. Zool.*, 1979, **209**, 115–127.
8 L. Hinkle, C. D. McCaig and K. R. Robinson, The direction of growth of differentiating neurones and myoblasts from frog embryos in an applied electric field, *J. Physiol.*, 1981, **314**, 121–135.
9 K. R. Robinson, The responses of cells to electrical fields: a review, *J. Cell Biol.*, 1985, **101**, 2023–2027.
10 K. Kawamura and Y. Kano, Electrical stimulation induces neurite outgrowth in PC12m3 cells via the p38 mitogen-

activated protein kinase pathway, *Neurosci. Lett.*, 2019, **698**, 81–84.
11 B. C. Thompson, *et al.*, Conducting polymers, dual neurotrophins and pulsed electrical stimulation — Dramatic effects on neurite outgrowth, *J. Controlled Release*, 2010, **141**, 161–167.
12 S. Han, *et al.*, Electrical stimulation accelerates neurite regeneration in axotomized dorsal root ganglion neurons by increasing MMP-2 expression, *Biochem. Biophys. Res. Commun.*, 2019, **508**, 348–353.
13 D. Khare, B. Basu and A. K. Dubey, Electrical stimulation and piezoelectric biomaterials for bone tissue engineering applications, *Biomaterials*, 2020, **258**, 120280.
14 L. Leppik, *et al.*, Combining electrical stimulation and tissue engineering to treat large bone defects in a rat model, *Sci. Rep.*, 2018, **8**, 6307.
15 S. Rangarajan, L. Madden and N. Bursac, Use of Flow, Electrical, and Mechanical Stimulation to Promote Engineering of Striated Muscles, *Ann. Biomed. Eng.*, 2014, **42**, 1391–1405.
16 P. H. Peckham and J. S. Knutson, Functional Electrical Stimulation for Neuromuscular Applications, *Annu. Rev. Biomed. Eng.*, 2005, **7**, 327–360.
17 C. Khouri, *et al.*, Hierarchical evaluation of electrical stimulation protocols for chronic wound healing: An effect size meta-analysis, *Wound Repair Regen.*, 2017, **25**, 883–891.
18 D. You, K. Li, W. Guo, G. Zhao and C. Fu, Poly (lactic-co-glycolic acid)/graphene oxide composites combined with electrical stimulation in wound healing: preparation and characterization, *Int. J. Nanomed.*, 2019, **14**, 7039–7052.
19 R. Luo, J. Dai, J. Zhang and Z. Li, Accelerated Skin Wound Healing by Electrical Stimulation, *Adv. Healthcare Mater.*, 2021, **10**, 2100557.
20 A. Abedin-Do, *et al.*, Electrical stimulation promotes the wound-healing properties of diabetic human skin fibroblasts, *J. Tissue Eng. Regener. Med.*, 2022, **16**, 643–652.
21 S. Snyder, C. DeJulius and R. K. Willits, Electrical Stimulation Increases Random Migration of Human Dermal Fibroblasts, *Ann. Biomed. Eng.*, 2017, **45**, 2049–2060.
22 C. Ott and T. Jung, The MyoPulser field stimulator, a do it yourself programmable electronic pacemaker for contracting cells and tissues, *Sci. Rep.*, 2023, **13**, 2461.
23 S. Gabetti, *et al.*, Versatile electrical stimulator for cardiac tissue engineering—Investigation of charge-balanced monophasic and biphasic electrical stimulations, *Front. Bioeng. Biotechnol.*, 2023, **10**, 1031183.
24 A. C. Vandergriff, M. T. Hensley and K. Cheng, Isolation and Cryopreservation of Neonatal Rat Cardiomyocytes, *J. Visualized Exp.*, 2015, 52726, DOI: **10.3791/52726**.
25 S. A. Vaez, *et al.*, The cardiac niche role in cardiomyocyte differentiation of rat bone marrow-derived stromal cells: comparison between static and microfluidic cell culture methods, *EXCLI J.*, 2018, **17**, 762–774, DOI: **10.17179/EXCLI2018-1539**.
26 J. Zhang, *et al.*, Differential Effects of Short Term Feeding of a Soy Protein Isolate Diet and Estrogen Treatment on Bone in the Pre-Pubertal Rat, *PLoS One*, 2012, **7**, e35736.
27 J.-P. Gratton, P. Bernatchez and W. C. Sessa, Caveolae and Caveolins in the Cardiovascular System, *Circ. Res.*, 2004, **94**, 1408–1417.
28 Clinical Cardiac Pacing, Defibrillation and Resynchronization Therapy, in *Clinical Cardiac Pacing, Defibrillation and Resynchronization Therapy*, ed. K. Ellenbogen, G. N. Kay, B. L. Wilkoff, C.-P. Lau and A. Auricchio, Elsevier, 2017, pp. 1211–1232, DOI: **10.1016/B978-0-323-37804-8.00052-3**.
29 *Cardiac Pacing and ICDs*, ed. K. A. Ellenbogen and K. Kaszala, John Wiley & Sons, Hoboken, NJ, 2020.
30 G. Gregoratos, *et al.*, ACC/AHA Guidelines for Implantation of Cardiac Pacemakers and Antiarrhythmia Devices: Executive Summary: A Report of the American College of Cardiology/American Heart Association Task Force on Practice Guidelines (Committee on Pacemaker Implantation), *Circulation*, 1998, **97**, 1325–1335.
31 G. Rackauskas, *et al.*, Subthreshold High-Frequency Electrical Field Stimulation Induces VEGF Expression in Cardiomyocytes, *Cell Transplant.*, 2015, **24**, 1653–1659.
32 Q. M. Chen and A. J. Maltagliati, Nrf2 at the heart of oxidative stress and cardiac protection, *Physiol. Genomics*, 2018, **50**, 77–97.
33 M. J. Morgan and Z. Liu, Crosstalk of reactive oxygen species and NF-κB signaling, *Cell Res.*, 2011, **21**, 103–115.
34 S. L. K. Bowers, Q. Meng and J. D. Molkentin, Fibroblasts orchestrate cellular crosstalk in the heart through the ECM, *Nat. Cardiovasc. Res.*, 2022, **1**, 312–321.
35 D. Fan, A. Takawale, J. Lee and Z. Kassiri, Cardiac fibroblasts, fibrosis and extracellular matrix remodeling in heart disease, *Fibrog. Tissue Repair*, 2012, **5**, 15.
36 R. S. Lodi, L. Xia, Y. Zhang and F. Liu, Evolving roles of cardiac fibroblasts in cardiogenesis and immunology, electrophysiology, and aging, *Rev. Cardiovasc. Med.*, 2021, **22**, 1173.
37 C. A. Souders, S. L. K. Bowers and T. A. Baudino, Cardiac Fibroblast: The Renaissance Cell, *Circ. Res.*, 2009, **105**, 1164–1176.
38 G. Krenning, E. M. Zeisberg and R. Kalluri, The origin of fibroblasts and mechanism of cardiac fibrosis, *J. Cell. Physiol.*, 2010, **225**, 631–637.
39 C. Fan, *et al.*, CHIR99021 and fibroblast growth factor 1 enhance the regenerative potency of human cardiac muscle patch after myocardial infarction in mice, *J. Mol. Cell. Cardiol.*, 2020, **141**, 1–10.
40 A. Kahn-Krell, *et al.*, A three-dimensional culture system for generating cardiac spheroids composed of cardiomyocytes, endothelial cells, smooth-muscle cells, and cardiac fibroblasts derived from human induced-pluripotent stem cells, *Front. Bioeng. Biotechnol.*, 2022, **10**, 908848.
41 Y. Zhu, *et al.*, Asparagine Synthetase Marks a Distinct Dependency Threshold for Cardiomyocyte Dedifferentiation, *Circulation*, 2024, **149**(23), DOI: **10.1161/CIRCULATIONAHA.123.063965**.
42 M. Szibor, J. Pöling, H. Warnecke, T. Kubin and T. Braun, Remodeling and dedifferentiation of adult cardiomyocytes during disease and regeneration, *Cell. Mol. Life Sci.*, 2014, **71**, 1907–1916.

43 Y.-Y. Cheng, *et al.*, Metabolic Changes Associated With Cardiomyocyte Dedifferentiation Enable Adult Mammalian Cardiac Regeneration, *Circulation*, 2022, **146**, 1950–1967.
44 L. Scott, K. Elídóttir, K. Jeevaratnam, I. Jurewicz and R. Lewis, Electrical stimulation through conductive scaffolds for cardiomyocyte tissue engineering: Systematic review and narrative synthesis, *Ann. N. Y. Acad. Sci.*, 2022, **1515**, 105–119.
45 X. Mei and K. Cheng, Recent Development in Therapeutic Cardiac Patches, *Front. Cardiovasc. Med.*, 2020, **7**, 610364.
46 D. Hernández, *et al.*, Electrical Stimulation Promotes Cardiac Differentiation of Human Induced Pluripotent Stem Cells, *Stem Cells Int.*, 2016, **2016**, 1–12.
47 S. Yoshida, K. Sumomozawa, K. Nagamine and M. Nishizawa, Hydrogel Microchambers Integrated with Organic Electrodes for Efficient Electrical Stimulation of Human iPSC-Derived Cardiomyocytes, *Macromol. Biosci.*, 2019, **19**, 1900060.
48 P. Syren, *et al.*, Heterogeneity of ventricular action potentials in neonatal rat cardiomyocytes and methodological aspects of patch clamp measurements, *Front. Physiol.*, 2025, **16**, 1537345.
49 M. Hoekstra, C. L. Mummery, A. A. M. Wilde, C. R. Bezzina and A. O. Verkerk, Induced pluripotent stem cell derived cardiomyocytes as models for cardiac arrhythmias, *Front. Physiol.*, 2012, **3**, 346.

